Reduced substrate clamping effect and evidence of shape memory behavior in vertically aligned Ni-Mn-In nanorod arrays

Kirandeep Singh, Shuvam Pawar, Davinder Kaur

Functional Nanomaterials Research Lab, Department of Physics and Centre of Nanotechnology, Indian Institute of Technology Roorkee, Uttarakhand, 247667, India

[*]Corresponding author, E-mail: dkaurfph@iitr.ac.in; Tel: (+91) 1332-2285407

Abstract

Silicon integrated vertically aligned Ni-Mn-In nanorod arrays having ~100 nm length were investigated for shape memory behavior and magnetocaloric effect. The room temperature X-ray diffraction (XRD) patterns revealed the (220) oriented pure austenitic cubic phase growth of Ni–Mn–In nanorods. The systematic thermo-magnetic (M-T) plots, resistance vs. temperature (R-T) measurements, as well as the negative slope of Arrott plots (H/M vs. M^2) curves revealed the existence of significant shape memory effect in 100 nm Ni-Mn-In rods between $230 \leq T \leq 294$ K region. The formation of narrow hysteresis between field cooled (FC) and field warm (FW) curves in contrast to previous studies which reported broadness in the martensitic transformation temperature regime with decreasing thickness [**1**], can be ascribed to reduced substrate clamping effect due to vertically aligned growth of Ni-Mn-In. The magnetocaloric curves evaluated from M-H study indicates that large magnetic field magnitude dependent entropy change occurs in Ni-Mn-In rods, a maximum attainable ΔS_M ~ 0.4 mJ/cc.K was observed at 275 K. Such vertically aligned growth of Ferromagnetic Shape Memory Alloys (FSMA's) thin films over semiconductor substrate exhibiting significant shape memory behavior could prove useful in many MEMS/NEMS applications as well as opens possibility of futuristic self-cooled spintronics devices like magneto-electric random access memory (ME-RAM). Copyright © 2016 VBRI Press.

Keywords: Thin films, X-ray diffraction, magneto-caloric, magnetization, nanorods.

Introduction

In recent years the multifunctional Heusler alloys exhibiting temperature, magnetic field as well as pressure controlled shape memory behavior, and several significant magneto responsive effects like: anomalous Hall effect, giant magnetocaloric effect, fast frequency response, etc, have received an ever increasing attention from both fundamental and material science community [**2,3,14**]. This concern has been sparked by their energy saving and environmental friendly technological applications such as: solid state magnetic refrigeration, magnetic actuators, sensors, energy harvesting devices, etc [**4,5**]. Such broad spectrum of ferromagnetic shape memory alloys (FSMA's) properties and applications is attributed to first order displacive, diffusionless solid to solid structural transition from high temperature austenitic cubic phase to lower symmetry (tetragonal, modulated orthorhombic, or monoclinic) phase occurred at a lower temperature. Till yet, most of the reported results on FSMA's have dealt with bulk, however, the synthesis of these materials in thin film form is essential **(i)** for the development of futuristic miniaturized electronic devices,

cooling devices, as well as nanoelectromechanical systems (NEMS) applications. Therefore, a comprehensive knowledge about thin film FSMA and how shape memory behavior changes at lower dimension compared to bulk is required. Theoretical and experimental investigation have shown that reduced dimension profoundly affects the microstructure of the material which in turn leads to significantly changed transformation behavior of FSMA's in thin films. The experimental studies on FSMA thin films conducted during last few years revealed that the grain size and film thickness have a profound effect on shape memory behavior in FSMA thin films. It was claimed by many researchers [**9**] that shape memory behavior vanishes at a significantly small thickness in polycrystalline FSMA thin films deposited on Si or other substrates. The recent reports by Auge at al. [**15**] and other groups claimed that only epitaxial utra thin films of FSMA's exhibits shape memory behavior. They also reported the broadness of transition regime and change in transition temperatures with lowering thickness [**1,6, 7, 16, 17**] in epitaxial ultra-thin films of off-stoichiometric Ni-Mn based Heusler

alloys. The factors like: substrate constraints, size scale effects, nucleus confinement, lattice mismatch induced stress strongly influenced the martensitic transformation characteristics of FSMA thin films [**1**]. However, at utra low thickness substrate constraints i.e. clamping of the functional behavior of FSMA by substrate due to its non-ferroic character and size effects were found to have a major impact on the shape memory behavior.

When dealing with thin films, the substrate plays a crucial role as it controls the texture and crystalline quality, therefore, the choice of worthy substrate for film growth is essential. Since silicon (Si) is the backbone of today's electronic industry, all the commercial devices are fabricated on Si. Therefore, to achieve the goal of commercializing FSMA based futuristic miniaturized commercial cooling devices, spintronics devices, NEMS, nano regime electronics, etc it is desirable to grow FSMA thin films on semiconductor substrates and to achieve shape memory behavior on those Si integrated thin films at low thickness. However, our recent studies on highly oriented Ni-Mn-In//Si ultra-thin films also reported the increased influence of substrate clamping effect on shape memory behavior at the reduced thickness and vanishing of twin variants actuations under external force (temperature, pressure, magnetic field) in ultralow thickness regime (< 30 nm) [**8**]. Therefore, in the present paper for the first time, an attempt has made to obtain the profound shape memory behavior in vertically aligned polycrystalline nanorods of $Ni_{50}Mn_{35}In_{15}$ grown on Si substrate by reducing the substrate originated constraints. To the best of our knowledge, no report is available in the literature on FSMA nanorods arrays grown on Si substrate by DC magnetron sputtering. This type of study will open up a new way for the utilization of these films in miniaturized spintronics devices, NEMS devices, stress sensors, transducers, etc.

Experimental

The vertically aligned Ni-Mn-In nanorod arrays were deposited using 50 mm × 3mm (diameter × thickness) 4N (99.9999 %) purity $Ni_{50}Mn_{35}In_{15}$ [Ni-Mn-In] commercial target (ACI Alloys Ltd.) by DC magnetron sputtering (Excel Mumbai, India) on (100) oriented highly doped P-type Si single crystal substrate maintained at a constant optimized temperature of $630^{o}C$. The Ni-Mn-In target was held at a distance of 27 cm from the substrate in on-axis sputter up geometry. The Si substrate was cleaned ultrasonically with equally weighted distilled water (resistivity ~ 20 MΩ. cm) and trichloroethylene (Alfa Aesar) mixture preceded by washing with boiled acetone (Alfa Aesar) and drying in N_2 atmosphere. Prior to fabrication of nanorods a very high vacuum with a base pressure ~ 4×10^{-7} Torr was achieved using turbomolecular pump backed by rotary vane pump. The deposition was carried out in 10 m Torr pure Ar atmosphere for 30 min at 80 W DC power supply. No post annealing treatment was provided to the Ni-Mn-In nanorods after deposition. The phase purity, crystallographic orientation and unit cell analysis of Ni-

Mn-In nanorods were analyzed by X-ray diffraction patterns collected in detector scan at 2° grazing angle using Bruker Advanced glancing angle X-ray diffractometer (GAXRD) equipped with CuKα radiations (1.54 A^{o}). The thickness and roughness studies of the films were carried out from cross-sectional micrographs collected using high resolution field emission electron microscopy (FE-SEM, FEI Quanta 200 model), and atomic force microscopy (AFM, NT-MDT INTEGRA model) respectively. The temperature and magnetic field driven shape memory behavior of the nanorods was tested by registering the temperature influenced resistance and thermomagnetic curves in 10 - 300 K range using helium compressed cryohead integrated with Keithley 2400 sourcemeter, 2182 nanovoltmeter and cryo free vibrating sample magnetometer (VSM, Cryogenics Ltd.) respectively. The isothermal magnetization data was recorded in ±0.2 Tesla magnetic field range and at different temperatures falling in the transition regime of the Ni-Mn-In. The cooling efficiency of these nanorods was tested through magnetocaloric studies.

Results and discussion

Fig. 1 shows the room temperature GAXRD of Ni-Mn-In nanorods obtained at 2° grazing angle in 10-70° 2(θ) range using slow scan speed of 1°/min. The existence of broad and highly intense (220) peak centered at 2(θ) ~ 42° along with appearance of (i) even lattice indexed peaks (200), (400) at 31.2^{o} and 62.3^{o} respectively, which follow $h+k+l= 2n$ law (n= integer) [**9**], and (ii) odd miller indices peaks (311) at 52.1^{o} which obeys $h+k+l=2n+1$ [**9**], confirms the pure austenitic cubic phase growth (L2$_1$) of Ni-Mn-In without any side phase.
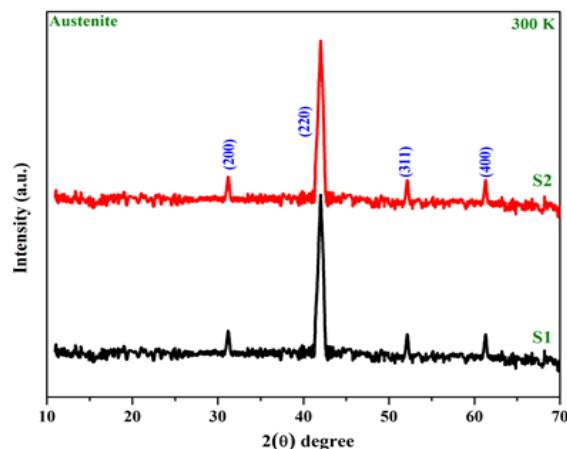

Fig. 1. Room temperature XRD patterns of S1 and S2 in 10-70° 2(θ) range.

The texture coefficient (TC) and substrate imposed strain 'ε' calculations was carried out using following equations to determine the crystallinity and nature of force between the substrate and Ni-Mn-In rods respectively.

$$TC(hkl)=\frac{I\ (hkl)}{\sum I\ (hkl)} \quad\quad\quad (1)$$

$$\epsilon = \left[\frac{(a-a_0)}{a_0} \right] \tag{2}$$

where, *I(hkl)* denotes the diffraction intensity of *hkl* reflection, '*a*' corresponds to lattice constant of strained thin film/nanorods, a_0 is the lattice parameter of bulk Ni-Mn-In (a_0=5.991 A°) [10] with same composition. A high texture coefficient ~74% value for (220) reflection authenticate the highly oriented and crystalline growth of Ni-Mn-In thin film. In addition, a low magnitudinal positive value of ε ~ 0.45 % revealed (i) the tensile nature of strain, (ii) rods are partially relaxed at the interface, (iii) presence of cohesive force at Ni-Mn-In rod and substrate interface. The above XRD results also revealed that 630°C substrate temperature (T_s) was proved to be optimum in terms of structural integrity and high crystallinity. The plane-view images along with the crosssectional micrographs were collected using high resolution FE-SEM and AFM (**Fig. 2**) to determine the microstructure and length of Ni-Mn-In rods, as well as to validate their vertical alignment.
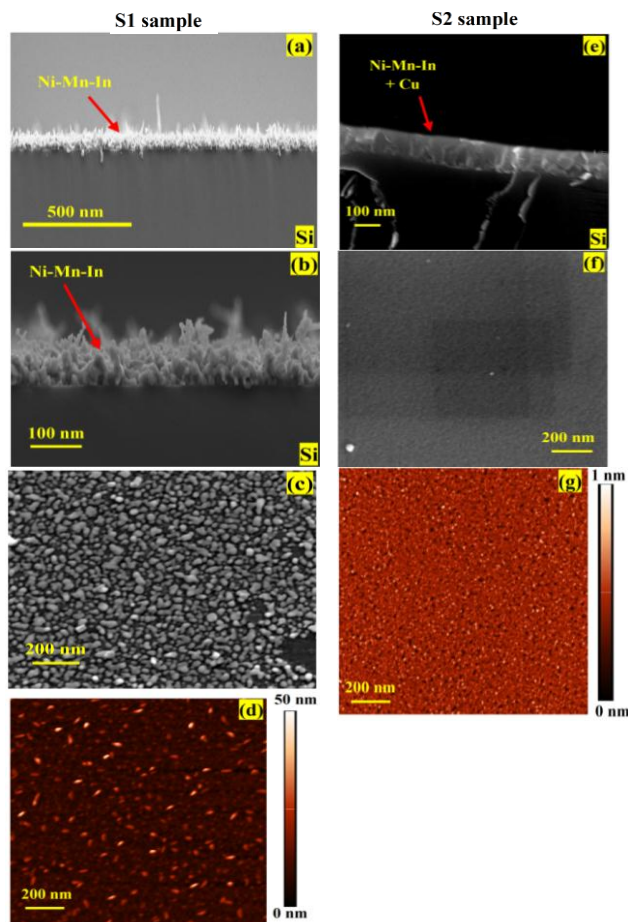

Fig. 2. Cross sectional FE-SEM micrographs, along with surface morphology, and roughness analysis of S1 and S2 samples.

The cross sectional FE-SEM studies authenticate the almost vertically aligned growth of Ni-Mn-In which are ~ 100 nm in length (calculated and reported after taking the mean) and it also revealed the formation of highly rough surface. The surface morphological images (top view of

Ni-Mn-In rods) collected using the FE-SEM and AFM again validate the highly rough surface, a surface roughness (root mean square roughness $R_{r.m.s.}$) ~ 20 nm was observed from the AFM measurements. However, such highly rough surface is not desirable and is disadvantageous for many CMOS integrated electronic applications. Thus, to reduce the roughness and to achieve a uniform and smooth surface, amorphous Cu (target maintained at 4.5 cm distance from the substrate) layer having ~ 20 nm thickness was deposited ex-situ on the top of the Ni-Mn-In nanorods, at room temperature in pure Ar atmosphere for 40 seconds using 50 W DC supply. The vertically aligned Ni-Mn-In nanorods with and without Cu layer will be abbreviated S1 and S2 hereon. The room temperature X-ray diffraction of the S2 sample performed at same conditions resembles exactly with S1 (**Fig. 1**), which confirms the amorphous growth of Cu on top of Ni-Mn-In at room temperature. The average surface roughness of the S2 sample as determine by AFM is less than 0.5 nm. The comparison of S1 and S2 FE-SEM cross-sectional micrographs indicates that the Cu layer filled the gaps between adjacent nanorods and it assists in achieving a uniform, smooth surface of Ni-Mn-In nanorods.

The temperature induced variation in the resistance along with thermo-magnetic curves of the samples S1 and S2 were recorded in cooling and heating mode in 70-300 K and 10 -300 K temperature range using helium compressed cryohead integrated with Keithley 2400 sourcemeter, 2182 nanovoltmeter and VSM respectively to confirm the presence of shape memory behaviour, to discover curie temperature (T_c), as well as to determine the temperature course during which Ni-Mn-In undergoes first order structural transformation, as shown in **Fig. 3**.
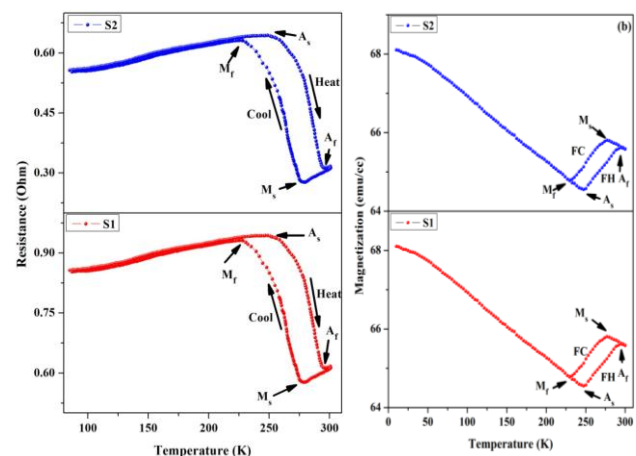

Fig. 3. Resistance vs. temperature and thermo-magnetic curves of S1 and S2 in 10-300 K and 80-300 K temperature respectively.

A delay of 30 seconds was provided before registering every data point to achieve the stationary equilibrium condition. The thermo-magnetic data of the samples collected at 0.01 T magnetic field was corrected using following equation to annihilate the contribution of Si substrate and top Cu layer which may affect the magnetic anisotropy of Ni-Mn-In nanorods.

$$M_{film}(H) = M_{total}(H) - \chi_{Substrate+Cu} . H \qquad (3)$$

where $\chi_{Substrate+Cu}$ is the susceptibility of the substrate and Cu layer, M_{total} is the total magnetization of the rods in combination with substrate and Cu layer, H is the magnetic field. The formation of thermal hysteresis between heating and cooling curves of M-T and R-T plots indicates the presence of shape memory behavior in Ni-Mn-In nanorods. Determined from cooling and heating curves the transformation temperatures (T_t) of S1 and S2 are found to be same i.e.: martensite start (M_s), martensite finish (M_f), austenite start (A_s), austenite finish (A_f) which are markers of transition regime occurs at: 280, 230, 248, 294 K respectively in both the samples. The narrower thermal hysteresis defined as: $\Delta T = (A_s + A_F)/2 - (M_s + M_f)/2$ between heating and cooling curves of S1 and S2 (~ 16 K) in contrast to our previous studies indicates the significant reduction of substrate clamping effect. From microscopic viewpoint, the occurrence of complicated thermal hysteresis in FSMA's is associated to nucleation of new phases as well as interfaces interaction with defects [17]. While, at mesoscopic level, creation, demolition, and redistribution of elastically interacting domains may be accountable for first order structural change in FSMA's [18]. Moreover, the generation of friction due to domain rearrangements can also contribute towards hysteresis. Below transition regime i.e. at T < 230 K, the rise in resistance followed by degradation of magnetic anisotropy with enhancement in measurement temperature signifies the normal ferromagnetic behavior of Ni-Mn-In nanorods. On, contrary the observable sharp decrease in resistance of Ni-Mn-In during transformation course can be ascribed to superzone boundary effect induced by structural superstructures and defects which led to an alteration in the density of states in the vicinity of Fermi surface [11,12]. In addition, the occurrence of large variation in magnetization of Ni-Mn-In during first order structural transformation may be due to (i) modification in Mn-Mn interatomic distance which in turn affects the exchange interaction [13], and (ii) formation of new crystallographic phases that temporarily disturbs the local ferromagnetic orientation [19]. The magnetic transition temperature (T_c) which in general was estimated using differentiation of M-T curves, was not observed in present Ni-Mn-In nanorods, due to no significant alteration in magnetic moment. The higher curie temperature value suggests that Ni-Mn-In nanorods are ferromagnetic at room temperature. The results of R-T and M-T plots also pointed out that (i) it is possible to tailor the transition regime of FSMA's by varying the degree of alignment of Ni-Mn-In rods, and (ii) shape memory may exist below 10 nm in fully vertically align Si integrated polycrystalline FSMA nanorods. The findings are promising for developing miniaturized electronics based on shape memory alloys thin films. The invariability in the transition regime of S1 and S2 indicates that top Cu layer doesn't affect the shape memory behavior of Ni-

Mn-In nanorods. The slight decrease in the resistance of S2 can be attributed to high conductivity of Cu in contrast to Ni-Mn-In. The occurrence of narrow hysteresis in present Ni-Mn-In nanorods likened to our previous reports on Ni-Mn-In ultrathin indicates that the difference in sample fabrication profoundly affects the phase transformation [8].

To test the cooling efficiency of S1 (M-H curve of S2 resembles similar to S1, not shown) iso-thermal magnetization curves was recorded in ± 0.2 T magnetic field range at different temperatures (falls in the transition regime) using loop process. The M-H curves were recorded in two steps, first, intensifying field mode (0T to 0.2 T), followed by decreasing the field intensity from 0.2 T to 0 T. The M-H data was registered at different temperatures, within the phase and well outside transition course of Ni-Mn-In nanorods. The M-H plot was collected by cooling the samples from 300 K to temperature of interest as shown in figure 4 and was used to calculate the entropy change. The metamagnetic like characteristics of field dependent magnetization loops at measured temperatures indicate the existence of shape memory behavior and ferromagnetic nature of vertically aligned Ni-Mn-In nanorods. To further validate the claim of first order structural transformation in present samples, Arrott plots (H/M vs M^2) was drawn using M-H curves, as shown in **Fig. 4**.
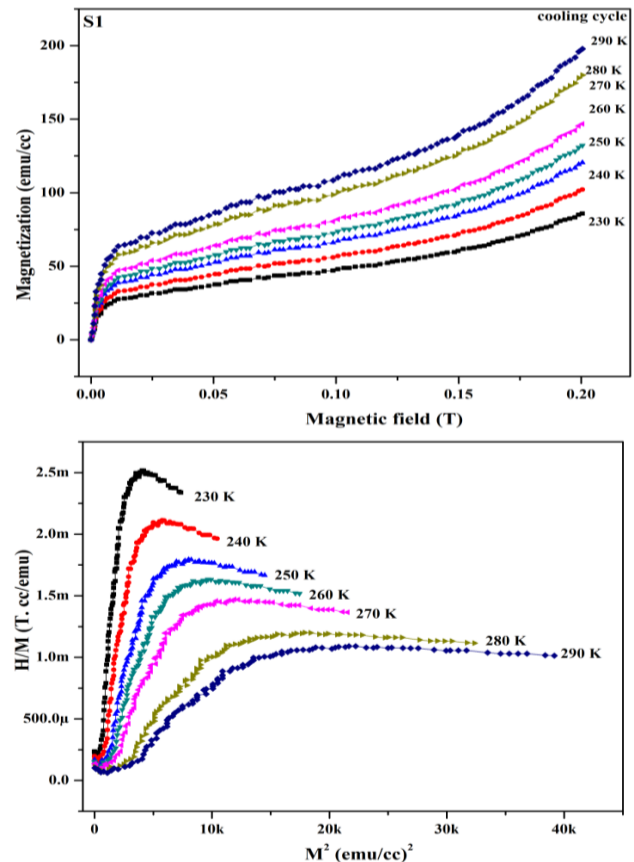

Fig. 4 Isothermal magnetization curves and Arrott plots of vertically aligned Ni-Mn-In nanorods.

The slope of Arrotts plots provides a metric to isolate first order structural transition from the normal magnetic transition of second order. The throughout positive slope of the Arrotts plots signifies ferromagnetic nature of the samples while shape memory behavior is indicated by their negative slope. Moreover, at Curie temperature the magnetic anisotropy drops to zero, as a consequence at $T=T_c$ the slope of H/M vs M^2 passes through the origin [**14**]. The appearance of negative slopes in S1 samples again confirms the presence of shape memory effect. Since, the Arrotts plots slope doesn't pass through the origin, it symbolizes the absence of T_c in Ni-Mn-In nanorods and their ferromagnetic nature at room temperature. The similar criterion to deduce the sequential transitions was utilized previously in Ni-Mn-Ga system [**20**].

A giant magnetic field dependent entropy change occurs in a system which endures first order structural transformation with concomitant magnetic ordering. Since, the magnetocaloric effect (MCE) is usually evaluated in terms of magnetic field driven isothermal entropy change (ΔS_M), a positive entropy changes means that samples cool down on the application of magnetic field, whereas, $\Delta S_M < 0$ signifies sample heats up under magnetic field. Thus, magnetic field induced (similar to isobaric) entropy change was calculated from isothermal M-H curves using Maxwell relation:

$$\Delta S_M(T,H) = \mu_0 \int_0^H \left[\frac{\partial M(T,H)}{\partial T}\right]_H dH \qquad (4)$$

The magnetic field driven entropy change in vertically aligned Ni-Mn-In nanorods is represented in **Fig. 5**. The positive peaks in ΔS_M indicate the inverse MCE and pointed out that samples cool under the application of external applied magnetic field.

Generally, The MCE is characterized by the full width at half maxima (FWHM) and apogee. A maximum entropy change of ~ 0.4 mJ/cc.K was observed around 275 K. The findings reveal the significance of these films in nano-length scale spot cooling.
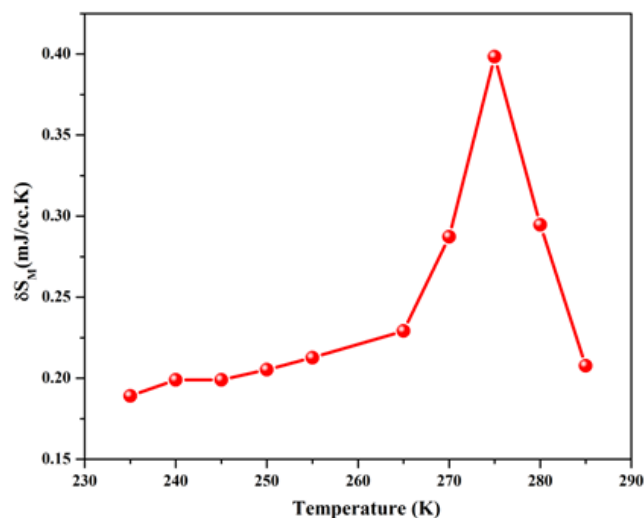

Fig. 5. Magnetic entropy variation of 100 nm Ni-Mn-In nanorods.

Conclusion

In conclusion, we have studied the vertically aligned highly rough Ni-Mn-In nanorods. The crystalline quality of the nanorods in austenite phase was quantified by texture coefficient (74% for (220) reflection) evaluated from XRD. The temperature driven resistance and magnetization changes along with negative slope of Arrotts plots indicate the presence of effective shape memory effect in Si integrated vertically aligned polycrystalline Ni-Mn-In nanorods. The validation of vertical alignment and degree of surface roughness in present high quality Ni-Mn-In nanorods was evaluated from cross-sectional FE-SEM micrographs and AFM images respectively. The positive peaks in isothermal entropy change vs. magnetic field plots revealed the significance of these nanorods in futuristic solid state magnetic refrigerators. The substrate clamping effect along with size effects are two important parameters which significantly reduced the actuation of twin variants under magnetic field at ultra-low thickness. However, the transition regime can be tuned at ultra-low regime by growing vertically aligned FSMA nanorods and by varying their degree of inclination. Based on our findings we suggested that such silicon integrated FSMA nanorods can pave a way for plenty of futuristic device application.

Author's Contributions

The author D.K. conceived the plan; The fabrication of samples, their characterization, data analysis as well as manuscript preparation was done by K. S.; The author S.P. presented the work at ICMTech 2016. Authors have no competing financial interests

References

1. Teichert, N.; Auge, A.; Yuzuak, E.; Dincer, I.; Elerman, Y.; Krumme, B.; Wende, H.; Yildirim, O.; Potzger, K.; Hutten, A. *Acta Mater.* **2015,** *86,* 279.
2. Dubenko, I.; Samanta, T.; Pathak, A.K.; Kazakov, A.; Prudnikov, V.; Stadler, S.; Granovsky, A.; Zhukov, A.; Ali, N. *J. Magn. Magn. Mater.* **2012,** *324,* 3530.
3. Liu, E.; Wang, W.; Feng, L.; Zhu, W.; Li, G.; Chen, J.; Zhang, H.; Wu, G.; Jiang, C.; Xu, H.; Boer, F. *Nat. Commun.* **2012,** *3,* 873.
4. Karaca, H.E.; Karaman, I.; Basaran, B.; Ren, Y.; Chumlyakov, Y.I.; Maier, H.J. *Adv. Funct. Mater.* **2009,** *19,* 983.
5. Sarawate, N.; Dapino, M. *Appl. Phys. Lett.* **2006,** *88,* 121923.
6. Sokolov, A.; Zhang, L.; Dubenko, I.; Samanta, T.; Stadler, S.; Ali, N. *Appl. Phys. Lett.* **2013,** *102,* 072407.
7. Ranzieri, P.; Fabbrici, S.; Nasi, L.; Righi, L.; Casoli, F.; Chernenko, V.A.; Villa, E.; Albertini, F. *Acta Mater.* **2013,** *61,* 263.
8. Singh, K.; Kaur, D. *Sens. Actuators, A.* **2015,** *236, 247*
9. Vishnoi, R.; Singhal, R.; Kaur, D. *J. Nanopart. Res.* **2011,** *13,* 3975.
10. Sunol, J.J.; Escoda, L.; Coll, R.; Saurina, J.; Sanchez, T.; Prida, V.M.; Hernando, B. *IOP Conf. Ser.: Mate. Sci. Eng.,* **2010,** *13,* 012004.
11. Zhang, B.; Zhang, X.X. ; Yu, S.Y.; Chen, J.L.; Cao, Z.X.; Wu, G.H. *Appl. Phys. Lett.* **2007,** *91,* 012510.

12. Antonov, V.N.; Perlov, A.Y. ; Oppeneer, P.M.; Yaresko, A.N.; Halilov, S.V. *Phys. Rev. Lett.* **1996,** *77,* 5253.
13. Das, R.; Perumal, A.; Srinivasan, A. *J. Alloys. Compd*. **2013,** *572,* 192.
14. Schwartz, W (Ed.); Encyclopedia of smart materials; Wiley: USA, **2002.**
15. Auge, A; Teichert, N; Meinert, M; Reiss, G; Hutten, A; Yuzuak, E; Dincer, I; Elerman, Y; Ennen, I; Schattschneider, Y *Phys. Rev. B*. **2012**, *85,* 214118.
16. Behler, A; Teichert, N; Dutta, B; Waske, A; Hickel, T; Auge, A; Hutten, A; Eckert, J. *AIP adv*. **2013**, *3,* 122112.
17. Das, R; Perumal, A; Srinivasan, A *J. Alloys Compd*. **2013**, *572,* 192.
18. Gao, B; Hu, H; Shen, J; Wang, J; Sun, J; Shen, B. *J. Appl. Phys*. **2009**, *105,* 083902.
19. Krenke, T; Acet, M; Wasserman, E; Moya, X; Manosa, L; Planes, A. *Phys. Rev. B*. **2006**, *73,* 174413.
20. Zhou, X; Li, W; Kunkel, H; Williams, G. *Phys. Rev. B*, **2006**, *73,* 012412.